Journal of Science and Technology in Civil Engineering, HUCE, 2025, 19 (2): 119–132

BUCKLING ANALYSIS OF GPL-REINFORCED FGM MICROPLATES USING PB-2 RITZ FUNCTIONS

Chu Thanh Binh[a,*]

[a]*Faculty of Building and Industrial Construction, Hanoi University of Civil Engineering, 55 Giai Phong road, Hai Ba Trung district, Hanoi, Vietnam*

Article history:
Received 03/3/2025, Revised 16/4/2025, Accepted 29/5/2025

Abstract

In this article, a buckling analysis of rectangular microplates under various boundary conditions is studied. The microplate is made of functionally graded material (FGM) reinforced with graphene nanoplatelets (GPLs). The FGM matrix is assumed to vary with the power-law distribution, while the GPLs are evenly distributed along the thickness. The modified Halpin-Tsai model and the rule of mixture are used to estimate the material properties of the GPL-reinforced FGM. The governing equation for the buckling problem of the microplate is developed using the modified couple stress theory (MCST), four-variable refined plate theory (RPT-4), and the pb-2 Ritz method. The solution is validated with those in existing literature, and the effects of different parameters (material characteristics, boundary conditions, size dependency, and geometric dimensions) on the critical buckling load of the microplate are given.

Keywords: buckling analysis; GPL-reinforced FGM; microplates; four-variable refined plate theory; modified couple stress theory (MCST); pb-2 Ritz method.

https://doi.org/10.31814/stce.huce2025-19(2)-09

1. Introduction

Nowadays, nano/microstructures are widely utilized in different fields such as electronics, automation, micro-electromechanical systems (MEMS), and nano-electromechanical systems (NEMS) [1, 2]. Among them, microbeam and microplate structures are crucial components of many microdevices. Therefore, studying the mechanical behaviors of microstructures is essential. Over the past decade, functionally graded materials (FGMs) composed of two constituent materials—ceramic and metal—have been a dominant research trend [3–6] due to their outstanding properties, such as high strength, high-temperature resistance, and corrosion resistance. Besides, the GPL-reinforced material model has also been widely used in recent years due to its superior mechanical, thermal, and electrical properties compared to conventional materials [7]. In the literature, most studies employ GPL reinforcement for isotropic or porous materials [7]. Recently, a FGM model reinforced by graphene platelets (GPLs) (i.e., GPL-FGM) was proposed [8], promising a potential research direction in recent years [9–12]. Thus, the present study will focus on analyzing a GPL-FGM microplate model.

In microstructure studies, two continuum theory models—the modified strain gradient theory (MSGT) and the modified couple stress theory (MCST) [13]—are commonly used in simulations. Among them, the MCST model, proposed by Yang et al. [14], is a simple and convenient theory as it requires only a single length-scale parameter to capture the size effects of microstructures. To solve small-scale issues, various size-dependent continuum models using the MCST are presented. For instance, utilizing the classical plate theory (CPT) and MCST, Yin et al. [15] and Jomehzadeh et al. [16] analyzed the free vibration behavior of isotropic microplates. Also, using classical plate

*Corresponding author. *E-mail address:* binhct@huce.edu.vn (Binh, C. T.)

theory (CPT)/first-order shear deformation (FSDT) and the MCST, Reddy and Berry [17] studied the axisymmetric bending behaviors of FGM microplates. Based on the Mindlin plate model and MCST, the mechanical behaviors of microplates were reported by Ke et al. [18] and Zhou and Gao [19]. Similarly, He et al. [20] presented buckling, bending, and free vibration analyses of the FGM microplate model using a four-unknown refined theory and the MCST. Also, utilizing the RPT-4 model, MCST, and Navier-type solution, Nguyen et al. [21] investigated the free vibration of FGM microplates placed on the Winkler-Pasternak elastic foundation. Recently, Nguyen and Chu [11] studied free vibration of GPL-FGM microplates on elastic foundations adopting the RPT-4 model and the MCST. It can be seen that many studies on the mechanical behavior of microplates have been reported in the existing literature [11, 22]. However, the buckling analysis for GPL-reinforced FGM microplates has not been explored.

Currently, higher-order shear deformation theories (HSDTs) have been widely used in the analysis of plate/shell structures [4]. According to these models, the in-plane displacement components are expressed as higher-order functions of the thickness coordinate. Essentially, HSDTs can provide more accurate results than classical plate theory (CPT) and first-order shear deformation theory (FSDT). Among HSDTs, the four-variable refined plate theory is a reasonable choice due to its simplicity and efficiency [23]. Therefore, to analyze microplate structures, the four-variable refined plate model (RPT-4) combined with the modified couple stress theory (MCST) is employed in the structural analysis presented in this paper.

In terms of computational methodology, although the pb-2 Ritz method has certain limitations, including dependence on the choice of trial functions and difficulty in application to problems with complex geometries or discontinuous boundary conditions, it is employed for the current problem due to several advantages, including high accuracy, applicability to various boundary conditions, and it does not require meshing like the finite element method (FEM).

Based on the above review, the present work focuses on the buckling analysis of an FGM microplate reinforced with GPLs (i.e., a GPL-FGM microplate). The governing equations for the buckling analysis are developed using the four-variable refined plate theory (RPT-4), the modified couple stress theory (MCST), as well as the pb-2 Ritz method. In the numerical results, the present findings are first verified with those in the existing literature. Then, the effects of material characteristics, boundary conditions, size dependency, and geometric dimensions on the critical buckling load of the microplates are analyzed.

2. Theoretical formulations

2.1. GPL-FGM microplate

Consider a rectangular microplate with a width of a, a length of b, and a thickness of h, in x-, y- and z-directions of the coordinate system, as indicated in Fig. 1. The microplate is made of new FGM reinforced by graphene platelets (GPLs). Note that the lower surface of the microplate is metal-rich, whereas the upper surface is ceramic-rich.

For the FGM matrix, material properties (i.e., elastic Young's modulus E_M, Poisson's ratio ν_M and mass density ρ_M) are assumed to vary following the power-law distribution along the thickness as follows [8]:

$$P_M(z) = (P_c - P_m)\left(\frac{z}{h} + \frac{1}{2}\right)^n + P_m \tag{1}$$

where n is the power-law index, P_c and P_m represent the material properties of the ceramic and metal constituents, respectively. The elastic Young's modulus of the composite (i.e., GPL-FGM) is

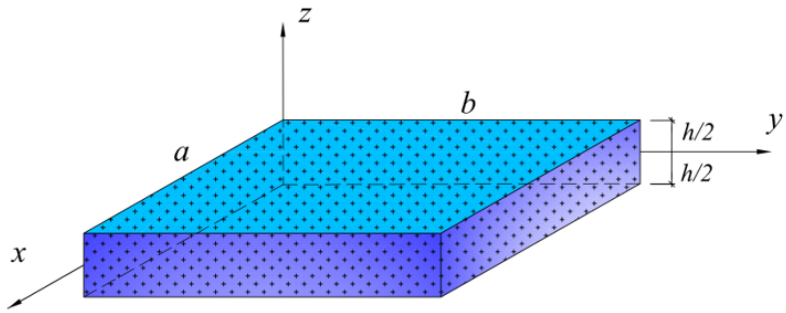

Figure 1. A GPL-reinforced FGM microplate

estimated using the modified Halpin-Tsai model as follows [7]:

$$E_c(z) = \left[\frac{3}{8}\frac{1+\overline{\xi}_{11}\overline{\eta}_{11}V_{gpl}(z)}{1-\overline{\eta}_{11}V_{gpl}(z)} + \frac{5}{8}\frac{1+\overline{\xi}_{22}\overline{\eta}_{22}V_{gpl}(z)}{1-\overline{\eta}_{22}V_{gpl}(z)}\right]E_M \tag{2}$$

Parameters $\overline{\eta}_{11}$, $\overline{\eta}_{22}$, $\overline{\xi}_{11}$, and $\overline{\xi}_{22}$ is computed by

$$\overline{\eta}_{11} = \frac{E_{gpl}-E_M}{E_{gpl}+\overline{\xi}_{11}E_M}; \quad \overline{\eta}_{22} = \frac{E_{gpl}-E_M}{E_{gpl}+\overline{\xi}_{22}E_M} \tag{3}$$

$$\overline{\xi}_{11} = 2\left(l_{gpl}/t_{gpl}\right); \quad \overline{\xi}_{22} = 2\left(b_{gpl}/t_{gpl}\right) \tag{4}$$

where E_{gpl}, l_{gpl}, b_{gpl}, and t_{gpl} are the elastic Young's modulus, average length, average width, and average thickness of the GPLs. The Poisson's ratio of the novel composite can be determined by [8]:

$$\nu_c(z) = \nu_{gpl}V_{gpl}(z) + \nu_M(z)\left[1-V_{gpl}(z)\right] \tag{5}$$

in which ν_{gpl} are the Poisson's ratio of the GPL. In the present study, the GPLs are assumed to be uniformly dispersed along the thickness, and the GPL volume fraction is determined as follows [8]:

$$V_{gpl}(z) = \frac{W_{gpl}}{W_{gpl}+\left(1-W_{gpl}\right)\rho_{gpl}/\hat{\rho}_M} \tag{6}$$

where $\hat{\rho}_M = \frac{1}{h}\int_{-\frac{h}{2}}^{\frac{h}{2}}\rho_M(z)\,dz$, and $\left(\rho_{gpl}, W_{gpl}\right)$ are mass density and the total weight fraction of the GPL.

2.2. Displacement, strain, stress components, and energy expressions

Based on the RPT-4 theory, the displacement components of the microplate are defined by [23]:

$$\begin{cases}\hat{u}(x,y,z) = u_0 - zw_{b,x} - f(z)\,w_{s,x}\\ \hat{v}(x,y,z) = v_0 - zw_{b,y} - f(z)\,w_{s,y}\\ \hat{w}(x,y,z) = w_b + w_s\end{cases} \tag{7}$$

where $\hat{u}, \hat{v}$ and $\hat{w}$ are the displacement components of a specific point in the microplate along the x, y, and z directions. Letters u_0, v_0 are the displacement components on the midplane along the x- and y-directions, respectively. w_b and w_s are the bending and shear components of the deflection

w. In this research, shear function $f(z) = \frac{3}{2}\left(\frac{z^3}{h^2}\right) - \frac{z}{8}$ is selected for buckling analysis. The linear strain-displacement relationships for the microplate are given by [23]:

$$\begin{Bmatrix} \varepsilon_{xx} \\ \varepsilon_{yy} \\ \gamma_{xy} \end{Bmatrix} = \begin{Bmatrix} \varepsilon^0_{xx} \\ \varepsilon^0_{yy} \\ \gamma^0_{xy} \end{Bmatrix} + z\begin{Bmatrix} k^b_{xx} \\ k^b_{yy} \\ k^b_{xy} \end{Bmatrix} + f(z)\begin{Bmatrix} k^s_{xx} \\ k^s_{yy} \\ k^s_{xy} \end{Bmatrix} \tag{8}$$

$$\begin{Bmatrix} \gamma_{yz} \\ \gamma_{xz} \end{Bmatrix} = g(z)\begin{Bmatrix} \gamma^s_{yz} \\ \gamma^s_{xz} \end{Bmatrix} \tag{9}$$

where

$$\begin{Bmatrix} \varepsilon^0_{xx} \\ \varepsilon^0_{yy} \\ \gamma^0_{xy} \end{Bmatrix} = \begin{Bmatrix} u_{0,x} \\ v_{0,y} \\ u_{0,y} + v_{0,x} \end{Bmatrix}; \quad \begin{Bmatrix} k^b_{xx} \\ k^b_{yy} \\ k^b_{xy} \end{Bmatrix} = \begin{Bmatrix} -w_{b,xx} \\ -w_{b,yy} \\ -2w_{b,xy} \end{Bmatrix}; \quad \begin{Bmatrix} k^s_{xx} \\ k^s_{yy} \\ k^s_{xy} \end{Bmatrix} = \begin{Bmatrix} -w_{s,xx} \\ -w_{s,yy} \\ -2w_{s,xy} \end{Bmatrix} \tag{10}$$

$$\begin{Bmatrix} \gamma^s_{yz} \\ \gamma^s_{xz} \end{Bmatrix} = \begin{Bmatrix} w_{s,y} \\ w_{s,x} \end{Bmatrix}; \quad g(z) = 1 - f'(z) \tag{11}$$

Based upon the MCST model, the components of the curvature tensor of the plate are as follows [11]:

$$\chi_{xx} = \chi^0_{xx} + (1 + f_{,z})\chi^1_{xx}; \quad \chi_{yy} = \chi^0_{yy} + (1 + f_{,z})\chi^1_{yy}; \quad \chi_{zz} = 0 \tag{12}$$

$$\chi_{xy} = \chi^0_{xy} + (1 + f_{,z})\chi^1_{xy}; \quad \chi_{yz} = \chi^0_{yz} + f_{,zz}\chi^1_{yz}; \quad \chi_{xz} = \chi^0_{xz} + f_{,zz}\chi^1_{xz} \tag{13}$$

in which

$$\chi^0_{xx} = w_{b,xy}; \quad \chi^1_{xx} = \frac{1}{2}w_{s,xy}; \quad \chi^0_{yy} = -w_{b,xy}; \quad \chi^1_{yy} = -\frac{1}{2}w_{s,xy} \tag{14}$$

$$\chi^0_{xy} = \frac{1}{2}\left(w_{b,yy} - w_{b,xx}\right); \quad \chi^1_{xy} = \frac{1}{4}\left(w_{s,yy} - w_{s,xx}\right) \tag{15}$$

$$\chi^0_{yz} = \frac{1}{4}\left(v_{0,xy} - u_{0,yy}\right); \quad \chi^1_{yz} = -\frac{1}{4}w_{s,x} \tag{16}$$

$$\chi^0_{xz} = \frac{1}{4}\left(v_{0,xx} - u_{0,xy}\right); \quad \chi^1_{xz} = \frac{1}{4}w_{s,y} \tag{17}$$

The stress-strain relationships in the microplate are defined by [24]:

$$\begin{Bmatrix} \sigma_{xx} \\ \sigma_{yy} \\ \sigma_{xy} \\ \sigma_{yz} \\ \sigma_{xz} \end{Bmatrix} = \begin{bmatrix} Q_{11} & Q_{12} & 0 & 0 & 0 \\ Q_{12} & Q_{22} & 0 & 0 & 0 \\ 0 & 0 & Q_{66} & 0 & 0 \\ 0 & 0 & 0 & Q_{44} & 0 \\ 0 & 0 & 0 & 0 & Q_{55} \end{bmatrix} \begin{Bmatrix} \varepsilon_{xx} \\ \varepsilon_{yy} \\ \gamma_{xy} \\ \gamma_{yz} \\ \gamma_{xz} \end{Bmatrix} \tag{18}$$

$$\begin{Bmatrix} t_{xx} \\ t_{yy} \\ t_{xy} \\ t_{yz} \\ t_{xz} \end{Bmatrix} = 2G_c l_0^2 \begin{bmatrix} 1 & 0 & 0 & 0 & 0 \\ 0 & 1 & 0 & 0 & 0 \\ 0 & 0 & 1 & 0 & 0 \\ 0 & 0 & 0 & 1 & 0 \\ 0 & 0 & 0 & 0 & 1 \end{bmatrix} \begin{Bmatrix} \chi_{xx} \\ \chi_{yy} \\ \chi_{xy} \\ \chi_{yz} \\ \chi_{xz} \end{Bmatrix} \tag{19}$$

in which l_0 is material length scale parameter, and non-zero coefficients Q_{ij} are provided as follows:

$$Q_{11} = Q_{22} = \frac{E_c(z)}{1-\nu_c^2(z)}; \quad Q_{12} = \frac{\nu_c(z)\,E_c(z)}{1-\nu_c^2(z)}; \quad Q_{66} = Q_{44} = Q_{55} = G_c = \frac{E_c(z)}{2\left[1+\nu_c(z)\right]} \tag{20}$$

The stress resultants in the microplate are defined by [20]:

$$\left(N_j, M_j^b, M_j^s\right) = \int_{-h/2}^{h/2} \sigma_j\,(1, z, f)\,dz; \quad j = xx, yy, xy \tag{21}$$

$$Q_j = \int_{-h/2}^{h/2} g\sigma_j dz; \quad j = yz, xz \tag{22}$$

$$P_j = \int_{-h/2}^{h/2} t_j dz; \quad j = xx, yy, xy, yz, xz \tag{23}$$

$$R_j = \int_{-h/2}^{h/2} (1+f_{,z})\,t_j dz; \quad j = xx, yy, xy \tag{24}$$

$$S_j = \int_{-h/2}^{h/2} f_{,zz} t_j dz; \quad j = yz, xz \tag{25}$$

The strain energy of the microplate model is determined by [20]:

$$\begin{aligned} U = \frac{1}{2}\int_S (&N_{xx}\varepsilon_{xx}^0 + N_{yy}\varepsilon_{yy}^0 + N_{xy}\gamma_{xy}^0 + M_{xx}^b k_{xx}^b + M_{yy}^b k_{yy}^b + M_{xy}^b k_{xy}^b + M_{xx}^s k_{xx}^s + M_{yy}^s k_{yy}^s \\ &+ M_{xy}^s k_{xy}^s + Q_{yz}\gamma_{yz}^s + Q_{xz}\gamma_{xz}^s + P_{xx}\chi_{xx}^0 + P_{yy}\chi_{yy}^0 + 2P_{xy}\chi_{xy}^0 + 2P_{yz}\chi_{yz}^0 + 2P_{xz}\chi_{xz}^0 \\ &+ R_{xx}\chi_{xx}^1 + R_{yy}\chi_{yy}^1 + 2R_{xy}\chi_{xy}^1 + 2S_{yz}\chi_{yz}^1 + 2S_{xz}\chi_{xz}^1)dS \end{aligned} \tag{26}$$

The potential energy of pre-buckling loads can be obtained as follows [25]

$$V = -\frac{1}{2}\int_S \left[N_{x0}\left(\frac{\partial \hat{w}}{\partial x}\right)^2 + N_{y0}\left(\frac{\partial \hat{w}}{\partial y}\right)^2 + 2N_{xy0}\frac{\partial \hat{w}}{\partial x}\frac{\partial \hat{w}}{\partial y}\right] dS \tag{27}$$

in which N_{x0}, N_{y0} and N_{xy0} are prebuckling in-plane normal and shear loadings. The total energy functional Π^* for buckling analysis can be determined by:

$$\Pi^* = U + V \tag{28}$$

3. Solution procedure

The GPL-FGM microplate is assumed to be subjected to in-plane loadings in two directions (bi-axial buckling), i.e., $N_{x0} = \gamma_1 N_0, N_{y0} = \gamma_2 N_0$, $N_{xy0} = 0$, as shown in Fig. 2.

For convenience, the following coordinate transformation is utilized:

$$\xi = \frac{2x}{a} - 1; \quad \eta = \frac{2y}{b} - 1 \tag{29}$$

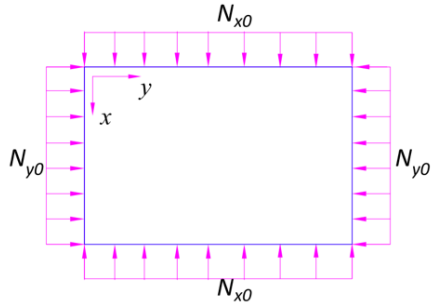

Figure 2. The GPL-FGM microplate model under a bi-axial compression

Using the pb-2 Ritz functions, the displacement components (u_0, v_0, w_b, w_s) of the microplate are assumed in the series as follows [26, 27]:

$$\begin{cases} u_0(x,y) = \sum_{p=0}^{N^*}\sum_{r=0}^{p} X_{pr}u_{pr}(\xi,\eta) = \sum_{i=1}^{M} X_i u_i(\xi,\eta) \\ v_0(x,y) = \sum_{p=0}^{N^*}\sum_{r=0}^{p} Y_{pr}v_{pr}(\xi,\eta) = \sum_{i=1}^{M} Y_i v_i(\xi,\eta) \\ w_b(x,y) = \sum_{p=0}^{N^*}\sum_{r=0}^{p} Z_{pr}w_{bpr}(\xi,\eta) = \sum_{i=1}^{M} Z_i w_{bi}(\xi,\eta) \\ w_s(x,y) = \sum_{p=0}^{N^*}\sum_{r=0}^{p} H_{pr}w_{spr}(\xi,\eta) = \sum_{i=1}^{M} H_i w_{si}(\xi,\eta) \end{cases} \tag{30}$$

where N^* is the order of the two-dimensional polynomial. Letters (X_i, Y_i, Z_i, H_i) are unknown coefficients of the series. For these coefficients, note that the number of terms M and their indexes i are computed by:

$$M = \frac{(N^*+1)(N^*+2)}{2}; \quad i = \frac{(p+1)(p+2)}{2} - (p-r) \tag{31}$$

Also, note that components $(u_i, v_i, w_{bi}, w_{si})$ are the pb2-Ritz functions as defined similarly in [27]. The governing equation of the buckling analysis of the microplate can be obtained by substituting Eq. (30) into the displacement form of Eq. (28) and then minimizing the total energy functional with respect to the coefficients, as follows [25]:

$$\frac{\partial \Pi^*}{\partial X_i} = \frac{\partial \Pi^*}{\partial Y_i} = \frac{\partial \Pi^*}{\partial Z_i} = \frac{\partial \Pi^*}{\partial H_i} = 0; \quad i = (1, 2, \ldots, M) \tag{32}$$

The governing equation for the buckling problem of the GPL-FGM microplate can be written in the following form:

$$(\boldsymbol{K} - N_0 \boldsymbol{V})\,\boldsymbol{q} = \boldsymbol{0} \tag{33}$$

where $\boldsymbol{K}$ and $\boldsymbol{V}$ are the elastic stiffness and geometric stiffness matrices, respectively, and $\boldsymbol{q} = \{X_1\ X_2\ \ldots\ X_M\ \ldots\ H_M\}^T$ is the unknown coefficient vector. By solving Eq. (33), the buckling load (N_0) of the GPL-FGM microplate model can be easily obtained. Note that the critical buckling load is the minimum among all buckling loads, i.e., $N_{cr} = \min(N_0)$.

4. Verification examples

Unless otherwise stated, in the next verifications and investigations, the FGM microplates made from metal/ceramic (Al/ZrO_2), with metal and ceramic material properties as $E_m = 70$ GPa, $\nu_m = 0.3, \rho_m = 2702$ kg/m^3 and $E_c = 151$ GPa, $\nu_c = 0.3, \rho_c = 3000$ kg/m^3, respectively. The GPL material parameters are used as $E_{gpl} = 1010$ GPa, $\rho_{gpl} = 1062.5$ kg/m^3, $\nu_{gpl} = 0.186, l_{gpl} = 3$ nm, $b_{gpl} = 1.8$ nm, and $t_{gpl} = 0.7$ nm [28]. In the present study, note that the GPLs are assumed to be uniformly dispersed along the thickness of the microplate. The material length scale parameter is assumed to be $l_0 = 17.6$ μm. The rectangular plate model with four edges, and boundary conditions of the plate are named following a counterclockwise sequence starting at the edge $y = 0$. For instance, the microplate with the CSSF boundary condition means that we have clamped (C) at $y = 0$, simply supported (S) at

$x = a$, simply supported (S) at $y = b$, and free (F) at $x = 0$. Besides, the following critical buckling load and buckling load parameters are utilized in the numerical analysis:

$$\overline{N}_{cr} = \frac{N_{cr}a^2}{E_m h^3}; \quad \overline{N}_0 = \frac{N_0 a^2}{E_m h^3} \tag{34}$$

The computational accuracy and stability of numerical solutions are considered first in this section. Some special cases of the microplate model are then compared with similar models in existing literature.

4.1. Convergence study

The convergence of the critical buckling load $\overline{N}_{cr}$ of the GPL-FGM (Al/ZnO_2) microplate is presented in Table 1, where the degree of the polynomial (N^*) of the series is increased from 3 to 8. The GPL-FGM microplate with the SSSS boundary condition and input parameters $n = 1$, $W_{gpl} = 1.5\%$, $b/a = 1$, and $a/h = 20$ are considered. The findings show that when increasing the N^*, the normalized critical buckling load $\overline{N}_{cr}$ of the microplate converges as $N^* \geq 6$, in both the uni-axial ($\gamma_1 = 0, \gamma_2 = 1$) and bi-axial ($\gamma_1 = 1, \gamma_2 = 1$) compression cases. Thus, to ensure the convergence, $N^* = 8$ will be chosen to conduct the numerical investigations.

Table 1. Convergence study of critical buckling load $\overline{N}_{cr}$ of GPL-FGM microplate

(γ_1, γ_2)	l_0/h	N^*					
		3	4	5	6	7	8
(0, 1)	0	6.2090	6.2060	6.2059	6.2059	6.2059	6.2059
	0.5	13.1113	13.1047	13.1046	13.1046	13.1046	13.1046
	1	33.8137	33.7964	33.7963	33.7963	33.7963	33.7963
(1, 1)	0	3.1045	3.1030	3.1029	3.1029	3.1029	3.1029
	0.5	6.5557	6.5524	6.5523	6.5523	6.5523	6.5523
	1	16.9069	16.8982	16.8982	16.8981	16.8981	16.8981

4.2. Buckling of FGM microplate

Table 2. The critical buckling load $\overline{N}_{cr}$ of the FGM microplate under a bi-axial compression ($\gamma_1 = 1, \gamma_2 = 1$)

n	Source	l_0/h					
		0	0.2	0.4	0.6	0.8	1
0	He et al. [20]	18.9243	21.7771	30.3324	44.5855	64.5348	90.1804
	Present	18.9243	21.7771	30.3324	44.5855	64.5348	90.1804
1	He et al. [20]	8.1142	9.6815	14.3832	22.2188	33.1882	47.2914
	Present	8.1142	9.6819	14.3846	22.2220	33.1938	47.3002
10	He et al. [20]	3.7450	4.2752	5.8505	8.4589	12.1011	16.7793
	Present	3.7450	4.2755	5.8514	8.4609	12.1047	16.7849

In this example, to validate the FGM microplate model, the normalized critical buckling loads, $\overline{N}_{cr} = N_{cr}a^2/\left(E_m h^3\right)$, of the FGM microplate under bi-axial compression ($\gamma_1 = 1, \gamma_2 = 1$) are compared with those of He et al. [20]. The FGM microplate model is composed of two constituent

materials (metal/ceramic) with $E_c = 14.4$ GPa, $E_m = 1.44$ GPa , and $\nu_c = \nu_m = 0.38$. The microplate has geometric dimensions of $a/b = 1$ and $a/h = 20$, while the ratio l_0/h and the power-law index n vary. The comparison between the two models are listed in Table 2. We can see that the discrepancy between the results of the present model and those of He et al. [20] using the Navier solution, the four-variable refined plate theory $\left(f = -\frac{z}{4} + \frac{5}{3}\frac{z^3}{h^2}\right)$, and MCST model is insignificant.

4.3. Buckling of GPL-reinforced macroplate

To validate the GPL-reinforced plate model, the normalized critical buckling load, $\tilde{N}_{cr} = N_{cr}\left(1-\nu_m^2\right)/\left(E_m h\right)$, of the GPL-reinforced plate under uni-axial compression ($\gamma_1 = 0, \gamma_2 = 1$) is compared with the results of Nguyen and Pham [29]. The macroplate is made of an isotropic matrix material with $E_m = 3$ GPa, $\rho_m = 1200$ kg/m^3, $\nu_m = 0.34$, and reinforced by GPLs with $E_{gpl} = 1010$ GPa, $\rho_{gpl} = 1062.5$ kg/m^3, $\nu_{gpl} = 0.186$ [29]. The plate has geometric dimensions of $a/b = 1$ and $a/h = 10$. The comparison results between the two models are shown in Table 3. It can be observed that the discrepancy between the results of the present model using the pb-2 Ritz method and those of Nguyen and Pham [29] using the isogeometric analysis (IGA) and the four-variable refined plate theory is insignificant in both SSSS and CCCC boundary conditions.

Table 3. The critical buckling load $\tilde{N}_{cr}$ of the GPL-reinforced plate under a uni-axial compression ($\gamma_1 = 0, \gamma_2 = 1$)

Boundary conditions	Source	W_{gpl} (%)			
		0	0.1	0.5	1
SSSS	Nguyen and Pham [29]	0.0310	0.0413	0.0825	0.1340
	Present	0.0310	0.0413	0.0825	0.1340
CCCC	Nguyen and Pham [29]	0.0692	0.0922	0.1841	0.2989
	Present	0.0692	0.0921	0.1839	0.2986

Through the above validation examples, we can observe that the present formulations and solutions are highly reliable. Therefore, further numerical investigations can be conducted to study the effects of parameters such as material properties, boundary conditions, size dependency, and geometric dimensions on the critical buckling load of the GPL-FGM microplates.

5. Parametric studies

In the next numerical investigations, the FGM model is made of Al/ZrO_2 reinforced with GPLs. It is also noted that the GPLs are assumed to be evenly distributed (uniformly dispersed) along the thickness of the microplate.

5.1. Influence of the GPL weight fraction

In this subsection, the influence of the GPL weight fraction (W_{gpl}) on the normalized buckling load $\overline{N}_0$ of the GPL-FGM microplate is investigated. Specifically, the variations of the $\overline{N}_o$ of the microplate under uni-axial and bi-axial compression are listed in Table 4 (Modes 1, 2, and 3) and shown in Fig. 3 (Mode 1). Three boundary conditions of the microplate are considered, including CCCC, CSCS, and SSSS. The microplate with input parameters $b/a = 1, a/h = 20, h/l_0 = 1$, and $n = 1$ is investigated.

We can see that the buckling load $\overline{N}_0$ of the GPL-FGM microplate gradually increases when the GPL weight fraction (W_{gpl}) rises, and this trend is quite consistent for both SSSS, CSCS, and

Table 4. The normalized buckling load $\overline{N}_0$ of the GPL-FGM microplate with different buckling modes

Case	Boundary condition	W_{gpl} (%)						
		0	0.5	1	1.5	2	2.5	3
Uni-axial compresion (Mode 1)	SSSS	29.254	30.771	32.285	33.796	35.305	36.812	38.317
	CSCS	49.062	51.603	54.139	56.672	59.201	61.726	64.247
	CCCC	72.769	76.540	80.306	84.065	87.819	91.567	95.309
Uni-axial compresion (Mode 2)	SSSS	45.327	47.676	50.021	52.363	54.701	57.036	59.367
	CSCS	74.578	78.442	82.300	86.152	89.998	93.838	97.673
	CCCC	83.144	87.452	91.754	96.050	100.338	104.621	108.896
Uni-axial compresion (Mode 3)	SSSS	79.475	83.594	87.706	91.812	95.911	100.005	104.092
	CSCS	128.111	134.747	141.374	147.991	154.598	161.196	167.783
	CCCC	136.907	144.000	151.083	158.155	165.216	172.267	179.308
Bi-axial compresion (Mode 1)	SSSS	14.627	15.385	16.142	16.898	17.653	18.406	19.158
	CSCS	27.891	29.336	30.778	32.217	33.655	35.090	36.523
	CCCC	38.431	40.423	42.411	44.397	46.380	48.359	50.335
Bi-axial compresion (Mode 2)	SSSS	36.261	38.141	40.017	41.891	43.761	45.629	47.494
	CSCS	42.878	45.098	47.316	49.530	51.740	53.948	56.152
	CCCC	66.890	70.356	73.817	77.272	80.723	84.168	87.608
Bi-axial compresion (Mode 3)	SSSS	36.261	38.141	40.017	41.891	43.761	45.629	47.494
	CSCS	61.906	65.113	68.316	71.513	74.706	77.894	81.077
	CCCC	66.890	70.356	73.817	77.272	80.723	84.168	87.608

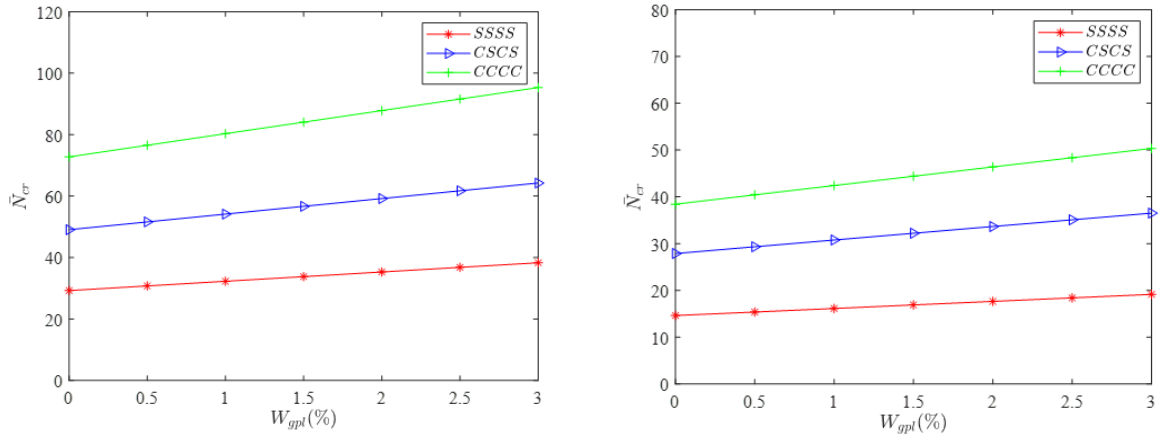

(a) Uni-axial compression

(b) Bi-axial compression

Figure 3. Variation of the critical buckling load $\overline{N}_{cr}$ of the GPL-FGM microplate with respect to W_{gpl} (Mode 1)

CCCC boundary conditions, as indicated in Table 4 and Fig. 3. For instance, as $W_{gpl} = 1.5\%$, the buckling load $\overline{N}_0$ of the GPL-FGM microplate increases by about 15.5%. As $W_{gpl} = 3\%$, the $\overline{N}_0$ of the microplate increases by about 31% compared to the case without the GPLs. This is due to the significantly higher stiffness of the GPLs compared to the FGM matrix, so even a small amount of

the GPLs makes a substantial increase in the stiffness of the microplate. The $\overline{N}_0$ of the microplate in the case of uni-axial buckling is higher than that in the case of bi-axial buckling.

5.2. *Influence of the boundary conditions*

In this subsection, the effect of the boundary conditions on the normalized critical buckling load $\overline{N}_{cr}$ of the GPL-FGM microplate is investigated. The critical buckling load $\overline{N}_{cr}$ of microplate under various boundary conditions (i.e., SSSS, CSCS, and CCCC) are illustrated for both uni-axial and bi-axial compression cases, as shown in Fig. 4(a) and Fig. 4(b), respectively. The microplate is under consideration with parameters $b/a = 1, a/h = 20, h/l_0 = 1, n = 1$, and $W_{gpl} = 1.5\%$.

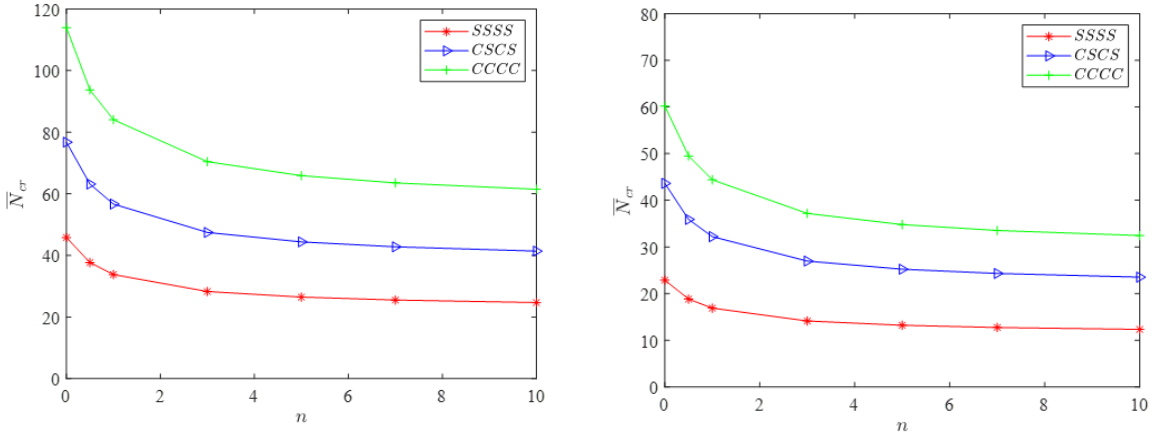

(a) Uni-axial compression

(b) Bi-axial compression

Figure 4. Variation of the critical buckling load $\overline{N}_{cr}$ of the GPL-reinforced FGM microplate with various boundary conditions

We can see that as the power-law index (n) increases, the normalized critical buckling load $\overline{N}_{cr}$ of the GPL-FGM microplate tends to vary in a similar manner across all boundary conditions investigated. The normalized critical buckling load $\overline{N}_{cr}$ of the microplate with the CCCC boundary condition is the highest, while that with the SSSS boundary condition is the lowest among them. This phenomenon occurs because the CCCC boundary condition significantly enhances the stiffness of the plate compared to other cases. Similarly, as the power-law index increases, the critical buckling load $\overline{N}_{cr}$ of microplates also decrease; it is significant when the power-law index is in the range of $0 < n < 3$.

5.3. *Influences of size dependency and power-law index*

The influences of the size dependency (h/l_0) and power-law index (n) on the normalized critical buckling load $\overline{N}_{cr}$ of the GPL-FGM microplate is investigated here. Specifically, the microplate is under SSSS boundary condition, and the input parameters as $b/a = 1, a/h = 20$, and $W_{gpl} = 1.5\%$ is considered. The power-law index n and the ratio h/l_0 are varied. The results for uni-axial and bi-axial compression cases are plotted in Fig. 5(a) and 5(b), respectively.

It can be observed that when the ratio h/l_0 decreases, the dimensions of the microplate become smaller, and the size-dependency effect on the $\overline{N}_{cr}$ of the microplate becomes very significant and more apparent. In contrast, when $h/l_0 > 10$, the $\overline{N}_{cr}$ of the microplate reduces very small, and indicating that the results of larger microplates go forward the buckling value and the behavior of the macroplate. When the index n increases (reducing the ceramic content), the $\overline{N}_{cr}$ of the microplate

decreases. This phenomenon occurs because the ceramic constituent is stiffer than the metallic constituent, thus, the stiffness of the microplate decreases when the ceramic content is decreased in the microplate.

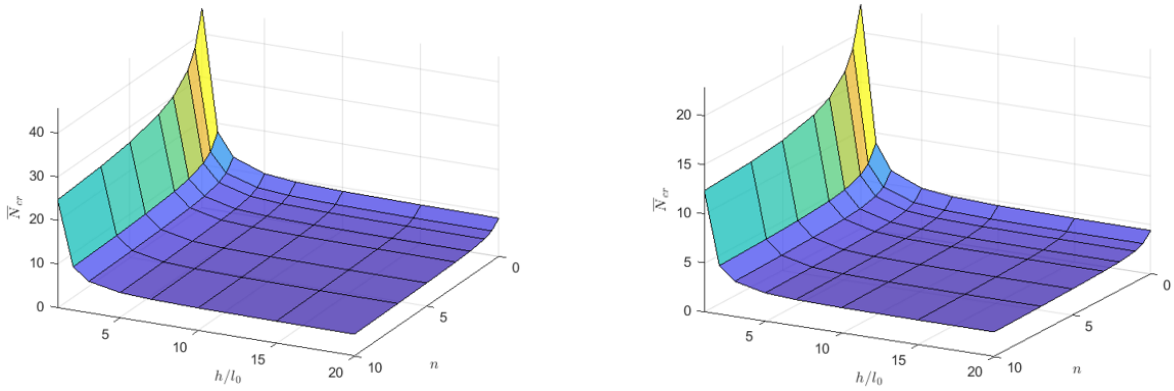

(a) Uni-axial compression (b) Bi-axial compression

Figure 5. Variation of the critical buckling load $\overline{N}_{cr}$ of the GPL-FGM microplates with respect to n and h/l_0

5.4. Influence of geometric dimensions

In this subsection, the influences of the aspect ratio (b/a) on the normalized critical buckling load $\overline{N}_{cr}$ of the GPL-FGM microplate is presented. The microplate under SSSS boundary condition, and the input parameters as $a/h = 20, h/l_0 = 1$ and $W_{gpl} = 1.5\%$ is considered. The results for uni-axial and bi-axial compression cases are plotted in Figs. 6(a) and 6(b), respectively. It can be observed that when the aspect ratio b/a increases, the normalized critical buckling load $\overline{N}_{cr}$ of the microplate generally tends to decrease. However, in the case of uni-axial compression, the graph exhibits a rather complex change consisting of multiple curves. This behavior is due to the mode buckling changes in the microplate as the ratio b/a increases. In contrast, for the case of bi-axial compression, the graph exhibits almost no mode change (resulting in a smooth curve) in the microplate occurring within the investigated range of $b/a = 0.5$ to 3.5. This trend remains consistent across all three cases $p = 0, 0.5$, and 1.

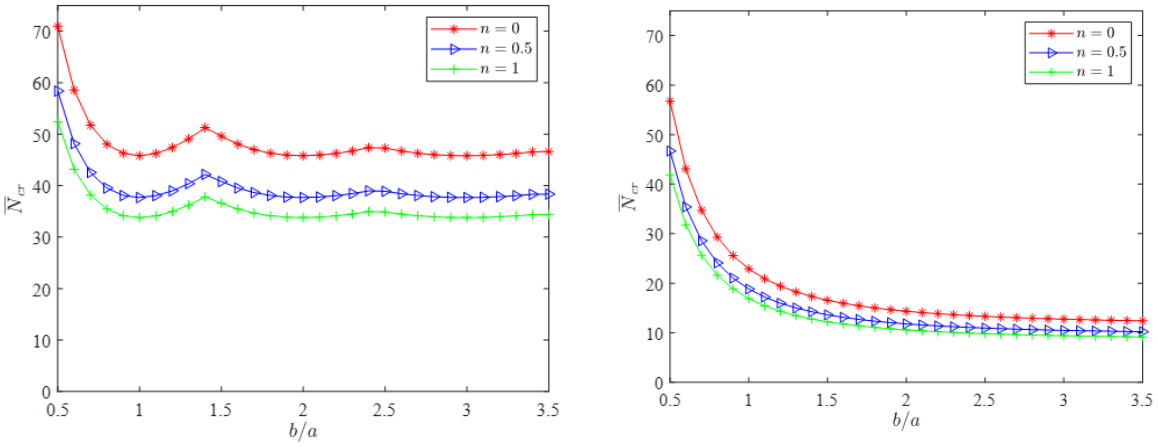

(a) Uni-axial compression ($l_0/h = 1$) (b) Bi-axial compression ($l_0/h = 1$)

Figure 6. Variation of the critical buckling load $\overline{N}_{cr}$ with respect to b/a

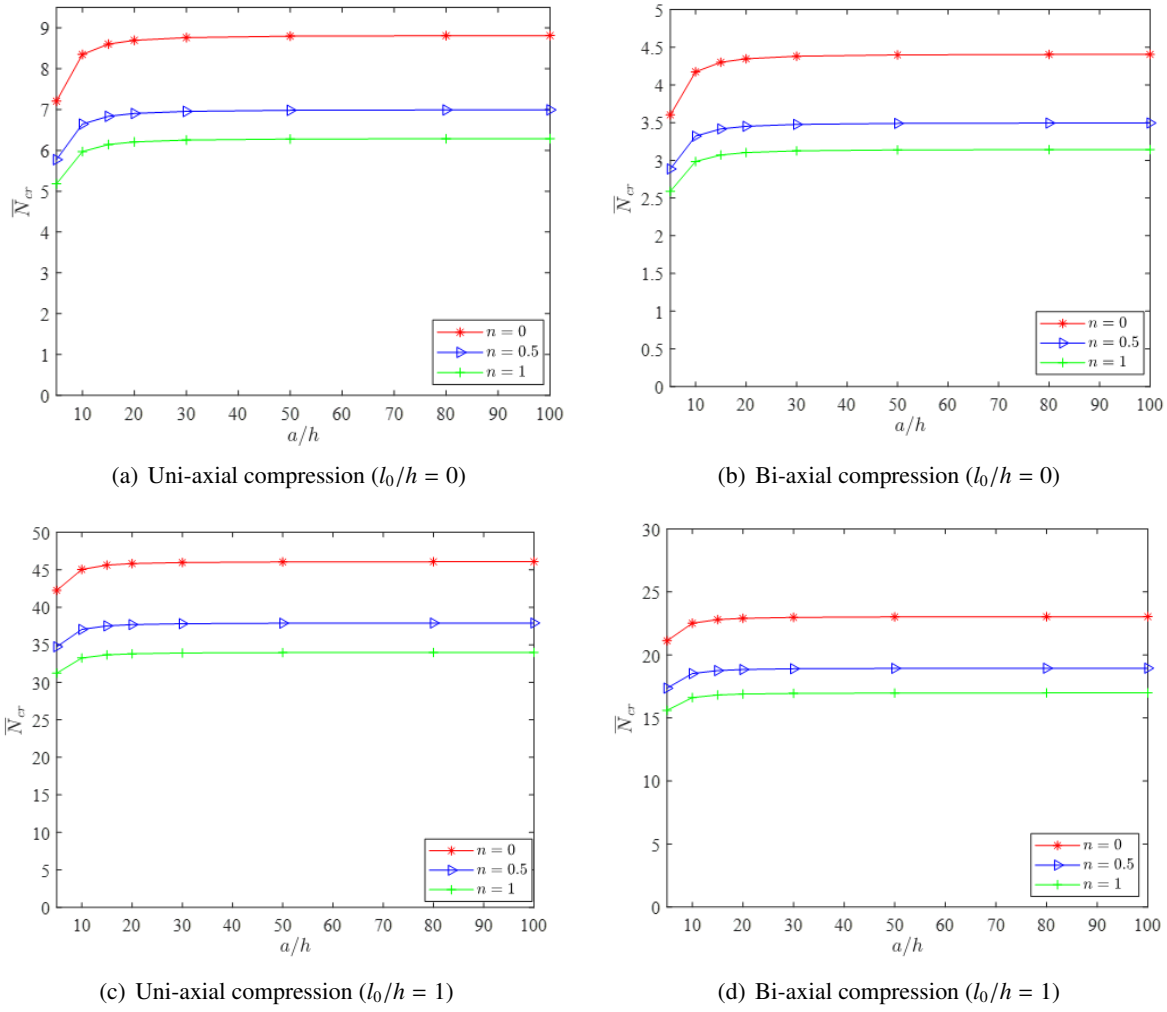

(a) Uni-axial compression ($l_0/h = 0$)

(b) Bi-axial compression ($l_0/h = 0$)

(c) Uni-axial compression ($l_0/h = 1$)

(d) Bi-axial compression ($l_0/h = 1$)

Figure 7. Variation of the critical buckling load $\overline{N}_{cr}$ with respect to a/h

Next, the influences of the thickness ratio (a/h) on the normalized critical buckling load $\overline{N}_{cr}$ of the GPL-FGM microplate is investigated. The microplate is under the SSSS boundary condition, and the input parameters as $b/a = 1$, and $W_{gpl} = 1.5\%$ is considered. The results of microplate under uni-axial and bi-axial compressions for the case $l_0/h = 0$ (traditional macroplate) are plotted in Figs. 7(a) and 7(b), and for the case $l_0/h = 1$ (microplate) of Figs. 7(c) and 7(d). The findings reveal that when the thickness ratio a/h increases, the normalized critical buckling load $\overline{N}_{cr}$ of the microplate tends to increase in all cases investigated. For example, for a macroplate ($l_0/h = 0$), the effect of the ratio a/h on the normalized critical buckling load is significant (with the plate at $a/h = 100$ experiencing an increase of approximately 21-24% compared to the case of $a/h = 5$). In contrast, for a microplate ($l_0/h = 1$), the effect of a/h on the normalized critical buckling load is much smaller (with the microplate at $a/h = 100$ increasing by only 8-9% compared to the case of $a/h = 5$). Clearly, the variation patterns of microplates are quite similar to those of traditional macroplates.

6. Conclusions

The paper presents the buckling analysis of the GPL-reinforced FGM microplates using the four-variable refined plate theory (RPT-4), the modified couple stress theory (MCST), and the pb-2 Ritz

method. Next, the numerical solution is verified with those of existing literature. The influences of parameters (n, W_{gpl}), size dependency (h/l_0), boundary conditions and geometric dimensions on the normalized critical buckling load of the microplates are investigated. Some key findings of the present study are provided below:

- When the GPL weight fraction (W_{gpl}) increases, the normalized critical buckling load $\overline{N}_{cr}$ of the GPL-FGM microplate significantly increases by about 31%, with $W_{gpl} = 3\%$, $n = 1$. In contrast, when the power-law index (n) increases, the normalized critical buckling load of the GPL-FGM microplates decreases.

- The normalized critical buckling load of the GPL-FGM microplate with CCCC boundary condition is higher than that of the microplate with SSSS, or CSCS boundary condition.

- When the ratio h/l_0 decreases, the dimensions of the microplate become smaller, and the size-dependency effect on the normalized critical buckling load $\overline{N}_{cr}$ of the GPL-FGM microplate becomes significant and more apparent. In contrast, when $h/l_0 > 10$, the $\overline{N}_{cr}$ of the microplate reduces very small, and indicating the results of larger microplates go forward the buckling value and the behavior of the macroplate.

- As anticipated, when the aspect ratio a/h is increased, or the ratio b/a is decreased, the normalized critical buckling load of the GPL-FGM microplate increases generally. The influence of the a/h ratio on the critical buckling load of the microplate is reduced compared to that of a conventional macroplate.

Acknowledgements

This research is funded by Ministry of Education and Training under grand number B2024.XDA.08.

References

[1] Tadigadapa, S., Mateti, K. (2009). Piezoelectric MEMS sensors: state-of-the-art and perspectives. *Measurement Science and Technology*, 20(9):092001.

[2] Hierold, C., Jungen, A., Stampfer, C., Helbling, T. (2007). Nano electromechanical sensors based on carbon nanotubes. *Sensors and Actuators A: Physical*, 136(1):51–61.

[3] Jha, D. K., Kant, T., Singh, R. K. (2013). A critical review of recent research on functionally graded plates. *Composite Structures*, 96:833–849.

[4] Thai, H.-T., Kim, S.-E. (2015). A review of theories for the modeling and analysis of functionally graded plates and shells. *Composite Structures*, 128:70–86.

[5] Nguyen, V.-L., Tran, B.-D., Chu, T.-B. (2018). Free vibration analysis of functionally graded cylindrical shell with stiffeners. *Journal of Science and Technology in Civil Engineering (STCE) - NUCE*, 12(6): 20–28. (in Vietnamese).

[6] Ghatage, P. S., Kar, V. R., Sudhagar, P. E. (2020). On the numerical modelling and analysis of multi-directional functionally graded composite structures: A review. *Composite Structures*, 236:111837.

[7] Zhao, S., Zhao, Z., Yang, Z., Ke, L., Kitipornchai, S., Yang, J. (2020). Functionally graded graphene reinforced composite structures: A review. *Engineering Structures*, 210:110339.

[8] Roun, S., Nguyen, V.-L., Rungamornrat, J. (2024). Free Vibration and Buckling Analyses of Functionally Graded Plates with Graphene Platelets Reinforcement. *Journal of Computing and Information Science in Engineering*, 25(1):011002.

[9] Nguyen, V.-L., Nguyen, V.-L., Tran, M.-T., Dang, X.-T. (2024). Investigation of static buckling and bending of nanoplates made of new functionally graded materials considering surface effects on an elastic foundation. *Acta Mechanica*, 235(12):7807–7833.

[10] Chu, T.-B., Nguyen, V.-L., Tran, M.-T., Nguyen, V.-L., Dang, X.-T. (2025). Free Vibration Analysis of Graphene-Reinforced FGM Nanoplates with Surface Energy Effects Resting on Elastic Foundation. *Iranian Journal of Science and Technology, Transactions of Mechanical Engineering*, 49(1):235–256.

[11] Loi, N. V., Binh, C. T. (2024). Free vibration analysis of graphene-reinforced FGM microplates under different boundary conditions. *The University of Danang - Journal of Science and Technology*, 70–76.

[12] Gawah, Q., Al-Osta, M. A., Bourada, F., Tounsi, A., Ahmad, S., Al-Zahrani, M. M. (2025). Bending analysis of graphene platelet-reinforced FG plates on Kerr foundations using an integral HSDT. *Acta Mechanica*, 236(3):1647–1671.

[13] Lien, T. V., Ha, L. T. (2024). Vibration analysis of Timoshenko microbeams made of functionally graded materials on a Winkler-Pasternak elastic foundation. *Vietnam Journal of Mechanics*, 46(1):31–43.

[14] Yang, F., Chong, A. C. M., Lam, D. C. C., Tong, P. (2002). Couple stress based strain gradient theory for elasticity. *International Journal of Solids and Structures*, 39(10):2731–2743.

[15] Yin, L., Qian, Q., Wang, L., Xia, W. (2010). Vibration analysis of microscale plates based on modified couple stress theory. *Acta Mechanica Solida Sinica*, 23(5):386–393.

[16] Jomehzadeh, E., Noori, H. R., Saidi, A. R. (2011). The size-dependent vibration analysis of micro-plates based on a modified couple stress theory. *Physica E: Low-dimensional Systems and Nanostructures*, 43 (4):877–883.

[17] Reddy, J. N., Berry, J. (2012). Nonlinear theories of axisymmetric bending of functionally graded circular plates with modified couple stress. *Composite Structures*, 94(12):3664–3668.

[18] Ke, L.-L., Wang, Y.-S., Yang, J., Kitipornchai, S. (2012). Free vibration of size-dependent Mindlin microplates based on the modified couple stress theory. *Journal of Sound and Vibration*, 331(1):94–106.

[19] Zhou, S.-S., Gao, X.-L. (2014). A Nonclassical Model for Circular Mindlin Plates Based on a Modified Couple Stress Theory. *Journal of Applied Mechanics*, 81(5).

[20] He, L., Lou, J., Zhang, E., Wang, Y., Bai, Y. (2015). A size-dependent four variable refined plate model for functionally graded microplates based on modified couple stress theory. *Composite Structures*, 130: 107–115.

[21] Nguyen, V.-L., Dang, X.-H., Doan, Q.-C. (2024). Free vibration of FGM microplates resting on elastic foundation. *Journal of Science and Technology in Civil Engineering (JSTCE) - HUCE*, 18(3V):34–47. (in Vietnamese).

[22] Yee, K., Ghayesh, M. H. (2023). A review on the mechanics of graphene nanoplatelets reinforced structures. *International Journal of Engineering Science*, 186:103831.

[23] Tran, H.-Q., Vu, V.-T., Tran, M.-T. (2023). Free vibration analysis of piezoelectric functionally graded porous plates with graphene platelets reinforcement by pb-2 Ritz method. *Composite Structures*, 305: 116535.

[24] Thai, H.-T., Kim, S.-E. (2013). A size-dependent functionally graded Reddy plate model based on a modified couple stress theory. *Composites Part B: Engineering*, 45(1):1636–1645.

[25] Yang, J., Chen, D., Kitipornchai, S. (2018). Buckling and free vibration analyses of functionally graded graphene reinforced porous nanocomposite plates based on Chebyshev-Ritz method. *Composite Structures*, 193:281–294.

[26] Wu, L. H., Lu, Y. (2011). Free vibration analysis of rectangular plates with internal columns and uniform elastic edge supports by pb-2 Ritz method. *International Journal of Mechanical Sciences*, 53(7):494–504.

[27] Nguyen, V.-L., Nguyen, V.-L., Nguyen, T.-A., Tran, M.-T. (2024). Dynamic responses of saturated functionally graded porous plates resting on elastic foundation and subjected to a moving mass using pb2-Ritz method. *Acta Mechanica*, 235(8):5301–5327.

[28] Arefi, M., Mohammad-Rezaei Bidgoli, E., Dimitri, R., Tornabene, F. (2018). Free vibrations of functionally graded polymer composite nanoplates reinforced with graphene nanoplatelets. *Aerospace Science and Technology*, 81:108–117.

[29] Nguyen, P.-C., Pham, Q.-H. (2023). A nonlocal isogeometric model for buckling and dynamic instability analyses of FG graphene platelets-reinforced nanoplates. *Materials Today Communications*, 34:105211.